

Revisions to the ASTER temperature/emissivity separation algorithm

William T. Gustafson, Alan R. Gillespie, and Gail J. Yamada

Department of Earth and Space Sciences

University of Washington

Seattle WA 98195-1310 USA

bill@rad.geology.washington.edu, arg3@u.washington.edu, gail@rad.geology.washington.edu

ABSTRACT - *The ASTER temperature/emissivity separation (TES) algorithm is used to make Standard Products containing surface temperature and emissivity images. It operates on land-leaving TIR radiance products, corrected for atmospheric transmissivity and sky radiance. Uncertainties have been attributed to 1) calibration, 2) atmospheric correction, and 3) measurement errors. Uncertainty is also introduced by an empirical power-law regression used to scale ASTER emissivity spectra. The 1- σ accuracy and precision were estimated at 1.5 K and 0.015, respectively, from models before the December 1999 launch of Terra and validated by field experiments. Later, however, errors of 4 K and scaling errors in emissivity were encountered in some images, especially in areas of low spectral contrast. We have undertaken to assess the magnitude and cause of this problem, and to rectify it if possible. It appears that errors in calibration and atmospheric compensation have led to over-correction for reflected downwelling irradiance and unacceptable errors in emissivity scaling. Serious inaccuracies occurred in ~4-5% of all frames, especially those taken near the ocean and with high atmospheric temperatures and humidity. Calibration errors have recently been reduced. Changes in TES have also improved the appearance of ASTER Standard Products: iterative correction for downwelling irradiance and the threshold test for spectral contrast have been removed. Although inaccuracies related to calibration, atmospheric compensation, and the TES regression remain, exaggeration of those inaccuracies by the algorithm has been reduced significantly.*

1 INTRODUCTION

There are more unknowns than measurements in thermal-infrared remote sensing, and temperature and emissivity separation is an underdetermined inversion. The solution is only as accurate as the independent constraints that can be applied, together with the limits imposed by measurement accuracy and precision. The independent constraints include atmospheric transmissivity and emission and, in the case of the ASTER temperature/emissivity separation (TES) algorithm, an empirical relationship between spectral emissivity (ϵ_λ) contrast (Gillespie *et al.*, 1998). In this paper we evaluate the TES algorithm and propose changes to improve performance.

The ASTER instrument was launched on NASA's Terra (EOS AM-1) spacecraft, in December 1999. The instrument contains three nadir-looking telescopes with three bands in the visible/near-infrared from 0.5-0.9 μ (VNIR), six in the short-wave infrared from 1.6-2.4 μ (SWIR) and five in the thermal infrared from 8-12 μ (TIR). One band on a fourth VNIR telescope looks back at 28.5° to get stereo data (Kahle *et al.*, 1991; Yamaguchi *et al.*, 1993).

The performance of the TES algorithm was evaluated using predicted values for sensor performance and atmospheric compensation, and tested on airborne TIR radiance data (Gillespie *et al.*,

1998). Some of these predictions have proven to be valid (instrument "noise"); for others the corrections have improved with experience (instrument calibration: Tonooka *et al.*, 2003). ASTER does not itself measure atmospheric characteristics, and for atmospheric compensation (Palluconi *et al.*, 1994, Thome *et al.*, 1998) used National Centers for Environmental Prediction (NCEP) Reanalysis data (<http://www.cdc.noaa.gov/cdc/reanalysis/reanalysis.shtml>) resampled from radiosonde atmospheric profiles of pressure, temperature, and relative humidity together with 1-km DEMs (Gesch and Larson, 1996) and MODTRAN 3.5 radiative transfer models (Abreu *et al.*, 1991, Anderson *et al.*, 1993) to estimate transmissivity, path spectral radiance, and downwelling spectral irradiance. This approach, based as it is on spatial-temporal interpolation, cannot reproduce differences at the edges of air masses, and it cannot be expected to result in accurate atmospheric compensation in all instances.

As we have gained experience with ASTER data we have proposed and implemented changes to the TES algorithm. This paper presents the reasoning for the proposed changes.

1.1 TES algorithm

TES is described in Gillespie *et al.* (1998). The key elements of the algorithm are summarized here. TES uses as input land-leaving spectral radiance and

downwelling spectral irradiance data that have been calibrated and compensated for atmospheric effects. TES uses the Normalized Emissivity Method (NEM: Gillespie, 1987) to estimate a model temperature, and an emissivity spectrum. The emissivities are used to compensate for reflected downwelling irradiance, assuming Kirchhoff's Law is applicable.

The NEM emissivities were calculated assuming that the maximum emissivity for the pixel spectrum is known *a priori*, and to the extent this assumption is not true the spectrum - and the NEM temperature - need to be rescaled. This is achieved using an empirical relationship between minimum emissivity ϵ_{\min} and emissivity contrast (Kealy and Hook, 1993), represented by the maximum spectral difference (MMD: Matsunaga, 1994). The MMD value is calculated for the normalized "Beta" spectrum, in which emissivity values are divided by their average value. Rescaling the Beta spectrum so that ϵ_{\min} equals the value from the regression yields the ASTER emissivity spectra and is used to calculate the surface temperatures. The ASTER regression is shown in Figure 1, and further comments are made here because of the importance of this regression to the problem.

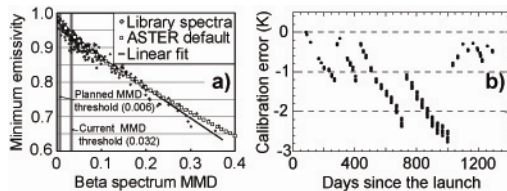


Figure 1. a) ASTER ϵ_{\min} vs. MMD regressions, for 250 library spectra. "ASTER default" is the power-law curve used in TES. "Linear fit" is its replacement. b) Sawtooth calibration pattern for ASTER Band 12 (after Tonooka *et al.*, 2003).

The ϵ_{\min} vs. MMD regression was based on data derived from a subset of the ASTER spectral library (<http://speclib@jpl.nasa.gov>) chosen to represent natural scene constituents. It is worth emphasizing that this editing was meaningful, because some have thought to improve the regression by including all spectra from the library, including those for metals, paints, and mineral cleavage faces that do not comprise significant fractions of most scenes. Even the edited library generates three classes of relationships in the ϵ_{\min} vs. MMD plane: spectrally flat materials such as vegetation, snow, and water cluster near unity on the ϵ_{\min} axis; soils plot on a line having low MMD values; and rocks plot on a different line and tend to have lower values of ϵ_{\min} and higher values of MMD than soils. Taken together, a power law is required to describe this behavior, and was adopted for the TES algorithm.

The power law underestimates the emissivity for water and vegetation and, because it slopes steeply for low values of MMD, tends to exaggerate measurement error "noise" for all low-contrast surfaces. This is especially pronounced for pixels affected by measurement error, which can only increase MMD (and therefore decrease ϵ_{\min}). To solve these problems, the scene was classified into low- and high-contrast pixels. Spectra with MMD values lower than a threshold value were assumed to be vegetation, and they were scaled so that their average values equaled the average value for vegetation. The planned threshold value was originally determined from the NEAT (<0.3 K: Fujisada, and Ono, 1993) and was MMD = 0.006; after ASTER spectra of water were found to have higher MMD values than predicted it was increased to MMD = 0.032.

Much of the excessive spectral variability appeared to be in Channel 10 (8.3 μm), the channel most strongly affected by atmospheric effects, and the most likely to be incorrectly compensated for them. Therefore, Channel 10 was excluded from the calculation of MMD, and a revised regression was used in TES.

Finally, because the rescaled emissivity spectra were more accurate than the NEM spectra, the land-leaving spectral radiance values were iteratively corrected for reflected downwelling spectral radiance, with a series of tests designed to determine when iteration should cease.

Gillespie *et al.* (1998) concluded that TES generated surface temperatures with 1- σ accuracies and precisions of 1.5 K, and emissivities with accuracies and precisions on 0.015. These uncertainties were caused in equal parts by measurement error (NEAT), errors in calibration, inaccurate atmospheric compensation, and natural variability in the spectral data used to determine the ϵ_{\min} vs. MMD regression.

1.2 Step discontinuities

The existence of step discontinuities due to the MMD threshold test were predicted when TES was designed. However, as experience was gained with the product they appeared to be more severe than predicted. Not only were water bodies and forests, but also soils and low-contrast rocks, as seen in Figure 2, which shows the effect for ASTER channel 12 over recent lava flows from Mauna Loa. Because the effect is due to a scaling problem, they affect all channels, as is shown in the TIR false-color figure in the Appendix. The severity of the problem is due to resetting the threshold from 0.006 to 0.032; however, step discontinuities occur in rock types that, according to the ASTER spectral library, should not be affected.

The step discontinuities are troubling because they disrupt the image for visual photo interpretation, they create local and unpredictable emissivity errors, and they create temperature errors. The last are especially troubling because many users are interested in water and canopy temperatures.

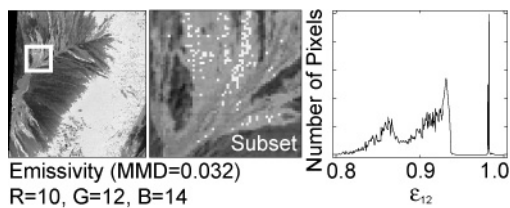


Figure 2. Spatial step discontinuities in a TES emissivity image (ASTER channel 12: 9.1 μm) of basalt flows on the island of Hawai'i with the MMD threshold value set to 0.032. a) Emissivity image. Rectangle is 64 90-m pixels (5.76 km) across. b) Subset from area of rectangle in a. c) Histogram of emissivities from the image subset. The gap and isolated spike in the histogram are due to the threshold test. In reality, the histogram should be continuous, with a tail out to 0.98. Because the emissivities are too high, temperatures are too low, by as much as 4 K.

2 APPROACH

Gillespie *et al.* (1998) suggested that the principal sources of error in TES products were errors in 1) calibration, 2) atmospheric compensation, including correction for downwelling irradiance, 3) measurement errors, and 4) natural variability in the ϵ_{min} v.s. MMD regression. In addition, of course, features of the algorithm itself, such as the successive estimation of the reflected downwelling term and the MMD threshold test, may contribute. In this assessment, we have examined calibration and atmospheric correction and their interactions with the TES code to explain the severity of the step discontinuities. We have excluded NEAT from consideration, because it is within design specifications Arai and Tonooka (2005) and was therefore considered before the release of TES products. We propose corrections to the algorithm and test them against the "problem" images to determine their effectiveness.

3 RESULTS

3.1 Extent of the problem

In a sample of a few hundred ASTER images, we found that only a few percent were affected by the step discontinuities - that is, in a few percent of the images the discontinuities occurred in rocky areas, or within water and/or forest areas instead of on their

boundaries, as was the plan for TES. However, we made the casual observation that the discontinuities appeared to be most common in low-altitude, warm-weather scenes.

3.2 Attribution of the problem

Calibration... It is anticipated that imaging systems such as ASTER change their sensitivity over time, and thus calibration coefficients used to convert measured signals into spectral radiances must be updated frequently. For ASTER, when radiance errors reached the 1% level for any channel, all the calibration coefficients were recomputed. This caused a sawtoothed pattern over time in spectral radiance accuracies (Fig. 1b).

By itself, the sawtoothed calibration pattern should not increase spectral contrast leading to the step discontinuities - the coefficients were updated before the inaccuracy exceeded the allowed-for 1%. However, the assumption had been that all channels changed sensitivity in a correlated way. This turned out not to be the case: different channels lost sensitivity at different rates, and the result was that although absolute calibration was within the specified limits, the relative accuracy from channel to channel exceeded expectation. Therefore, calibration errors could "color" the apparent emissivity spectrum, increasing the MMD and causing low-contrast spectra to be treated as high-contrast spectra inappropriately.

Tonooka *et al.* (2003) developed a new calibration correction that eliminates the sawtoothed pattern. This was done by fitting a curve to the calibration tests made over the 7-yr history of ASTER, and interpolating appropriate coefficients based on the number of days since launch. This improvement has been incorporated in the calibration software at The Eros Data Center (EDC) to produce the ASTER spectral radiance products.

Atmospheric correction... As described by Palluconi *et al.* (1994), ASTER atmospheric compensation is based on the NCEP water and temperature profiles which are resampled in time (6 hr) and space (1°) from data collected by weather balloons launched twice daily from more than 100 sites around the world. Surface barometric pressure is calculated from NCEP profiles and surface elevations taken from a 1-km digital elevation model. These profiles are used to set the initial conditions for MODTRAN models which generate the atmosphere transmissivity, upwelling spectral radiance, and downwelling spectral irradiance data used to calculate the TES input data.

Because the spectra of atmospheric transmissivity, path radiance, and downwelling spectral irradiance are strong functions of wavelength, even a constant fractional error in them has the potential of increasing the MMD of the surface emissivity spectrum. To the extent that the errors are decorrelated, that potential is even greater.

The atmospheric compensation appears to work within specifications most of the time, but the potential for occasional error is present. Probably most serious is the undersampling of moving air masses, which can lead to local errors. However, neither the variable boundary layer nor variable aerosol effects are considered in calculating the atmospheric parameters, and these oversights may increase compensation errors.

Hypothesizing that the errors in atmospheric compensation are proportional to the magnitude of the correction, we created a database of nominally cloud-free images of water bodies at different elevations (Table 1) to gain insight into the relationship between the occurrence of step discontinuities and irradiance. Water bodies are useful for this test because the emissivities are well-known already. We counted the number of step discontinuities in a 32x32 pixel subset of each image. Percent error was based on how many of the 1024 pixels were misclassified as rock by MMD threshold portion of the TES algorithm.

Scene	Lat, °N	Long, °E	Elev, m	Number of images
Salton Sea	33N	116W	-69	5
Hawaii	19N	155W	0	20
Lake Baikal	52N	104E	444	7
Lake Tahoe	39N	120W	1901	57
Koko Nur	37N	100E	3193	5

Table 1. Images of water used to estimate step-discontinuity error rates and test sensitivity to atmospheric compensation.

The percent error rate is shown in Figure 3 as a function of downwelling spectral irradiance, a measure of the magnitude of atmospheric correction. In general, the atmosphere above high-altitude lakes such as Koko Nur (Qinghai Lake) or Lake Tahoe can be expected to contain less water than above low-elevation lakes such as the Salton Sea.

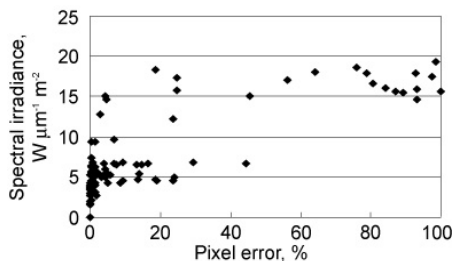


Figure 3. Channel 10 downwelling spectral radiance ($W \mu m^{-1} m^{-2}$) vs. percent pixel error.

The step-discontinuity rate does vary inversely with elevation, but the correlation is low. It is clear

that this relationship explains only a fraction of the variability, and that other factors are at work.

4 DISCUSSION

4.1 Calibration

Early in the mission, infrequent updating of calibration coefficients, together with the unexpected differences in detector sensitivity changes from channel to channel, caused graybodies to appear more strongly colored than they should, and the MMD threshold test to classify neighboring pixels of the same material differently due to normal changes in MMD brought about by normal measurement noise. However, improvements to the protocol since 2004 have removed calibration as a source of step discontinuities for images recently processed to land-leaving spectral radiance since 2005.

4.2 Atmospheric compensation

Because atmospheric transmission and emission terms are colored, uncompensated atmospheric contributions tend to give spectral radiance-at-sensor data higher MMD values than land-leaving spectral radiance. Proper conversion of land-leaving radiance to land-emitted spectral radiance by the subtraction of reflected downwelling spectral irradiance typically reduces MMD further. However, incorrect characterization of atmospheric parameters will leave the presumed land-emitted spectral radiance with higher spectral contrast than appropriate. By itself or in combination with calibration errors, this will cause the MMD threshold test to misclassify scene elements, leading to step discontinuities in the image.

It is reasonable that the effects of inaccurate atmospheric compensation may be complicated. Compensation for transmissivity and path spectral radiance is with a simple linear equation in each channel, but for irradiance - especially in TES - is iterative and depends on prior estimates of emissivity, which may already be in error. Under nominal conditions, the iterative correction can converge on a correct answer, but if the *a priori* estimate of emissivity, which includes the potential inaccuracies introduced in applying the linear compensation equation, is too low, the reflected irradiance term will be erroneously large, potentially leading to non-convergence, erroneously low final emissivity estimates, and high values of MMD.

4.2 MMD threshold test

When it became clear that graybodies were being classified incorrectly, the MMD threshold was increased from 0.006 to 0.032. However, this correction was unsatisfactory, because the errors in the TES input data were constantly changing. As shown

in Figures 1 and 2, increasing the MMD threshold caused misclassifying of surfaces as near-graybody.

4.3 Channel 10

Spectral effects of incorrect atmospheric compensation are most noticeable in channel 10, which at $8.4 \mu\text{m}$ is close to atmospheric water bands. In an effort to reduce the incidence of unrealistically high MMD values, MMD was calculated only for channels 11-14, and the power-law regression was revised accordingly. This revision appears to have been successful, and has been incorporated in TES.

4.4 New recommendations

MMD threshold... The classification of pixels into categories of low- and high-contrast using the MMD threshold has proven unsatisfactory, and we recommended removing it. This has the consequence of typically underestimating graybody emissivity (increasing apparent temperature) or greatly increasing emissivity uncertainty, due to the steepness of the power-law curve for low values of MMD. The increased uncertainty leads to "speckling" in the TES products. Therefore, we also have recommended replacing the power-law curve with the linear regression shown in Figure 1. This does not solve the underestimation problem, but at least does not increase the uncertainty. Figure 4 shows the improvement in appearance, and the emissivity histogram, due to this change on the Hawai'i image of Figure 2.

Irradiance correction... The iterative algorithm for the removal of spectral irradiance in TES fails frequently, probably due to inaccurate atmospheric correction, and should be eliminated. Only the nominal correction should be retained. This will enhance the emissivity recovery for non-gray body surfaces over the current method.

In-scene atmospheric correction... It appears that the atmosphere transmissivity and emission are sufficiently changeable that accurate temperature/emissivity recovery requires that they be measured at the time of image acquisition. MODIS data have the potential to serve in this capacity, at least for specifying total column water on a near pixel-by-pixel basis. It may also be possible to adapt an approach such as ISAC (Young *et al.*, 2002) to increase the accuracy of the shape of the recovered emissivity spectrum, although application to complex scenes containing soils and rocks as well as graybodies and accurate scaling of the emissivities requires independent scene classification such as used by the NDVI methods now (e.g., Sobrino *et al.*, 2001).

Temperatures for low-contrast scenes... Users interested in graybody (water, snow, or vegetation)

temperatures *per se* should examine the emissivity images (AST 05) prior to using the temperature data (AST 08). If the emissivity is incorrectly calculated then the temperatures will need to be calculated using Planck's Law. The spectral radiance data product (AST 9T) should be used as an input together with an assumed emissivity drawn for water, snow or vegetation from the ASTER spectral library. Because the emissivities are close to unity, correction for downwelling spectral irradiance is small may since the emissivities are known, it may be performed on the AST 9T data before application of Planck's Law. An independent separate classification of the scene using the VNIR bands or map data should be used to ensure that extracted temperatures are drawn from the correct material on the ground (Gustafson *et al.*, 2002).

5 CONCLUSIONS

The standard temperature and emissivity products for ASTER images contain artifactual step discontinuities that appear to result from imperfections in the atmospheric compensation that are exaggerated by the Temperature/ Emissivity Separation (TES) algorithm. These degrade the visual appearance of the images and interfere with photo interpretation. They may be removed by eliminating a classification into graybody/non-graybody scene elements that was originally introduced to make temperature recovery for water more accurate. Removal from TES of its iterative correction for reflected downwelling spectral irradiance will improve performance when atmospheric characterization is inaccurate.

Step discontinuities affect only a small fraction of the images acquired by ASTER and the temperature and emissivity standard products. In the majority of instances, TES works properly, within the accuracies and precisions estimated by Gillespie *et al.* (1998). The remedies we propose for the step-discontinuity problem will improve the appearance of all images, but at the expense of decreased precision and accuracy over graybody scenes such as water.

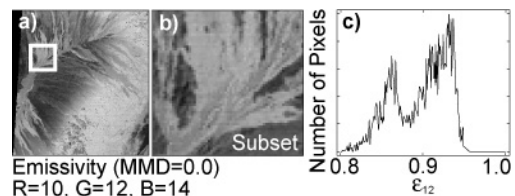


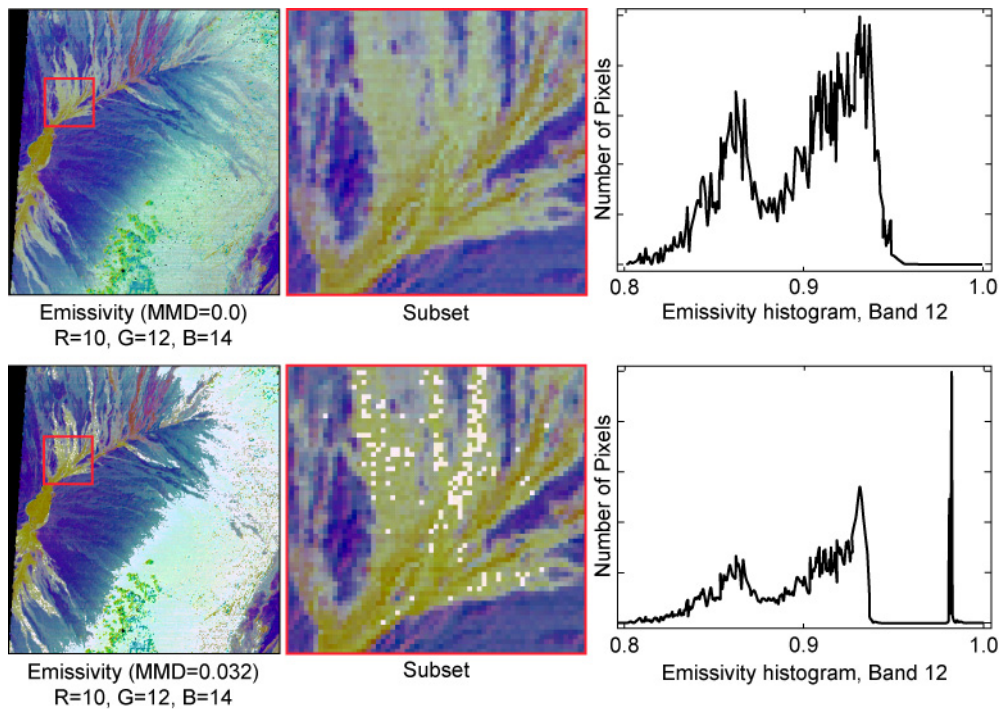
Figure 4. Removal of step discontinuities from ASTER emissivity data (Channel 12: $9.1 \mu\text{m}$) by setting the MMD threshold test to zero. Emissivity image. Rectangle is 64 90-m pixels (5.76 km) across. Image is the same as in Fig. 2. a) Emissivity image. b) Subset from area of rectangle in a. c) Histogram of emissivities from the image subset.

6 ACKNOWLEDGMENTS

This research was supported by NASA's ASTER program, contract NNG04HZ55c.

7 REFERENCES

- Abreu, L. W., F. X. Kneizys, G. P. Anderson, J. H. Chetwynd, A. Berk, L. S. Bernstein, and D. C. Robertson, 1991. MODTRAN. *The Proceedings of the 1991 Battlefield Atmospheric Conference*, (El Paso, TX).
- Anderson, G. P., J. H. Chetwynd, J.-M. Theriault, P. Acharya, A. Berk, D. C. Robertson, F. X. Kneizys, M. L. Hoke, L. W. Abreu, and E. P. Shettle, 1993. MODTRAN2: Suitability for Remote Sensing. *The workshop on atmospheric correction of Landsat Imagery*. Edited by P. N. Slater, L. D. Mendenhall. (Torrance, CA: Geodynamis Corporation).
- Arai, K., and Tonooka, H., 2005. Radiometric performance evaluation of ASTER VNIR, SWIR, and TIR, *IEEE Transactions on Geoscience and Remote Sensing*, 43, 2725-2732.
- Fujisada, H. and A. Ono, 1993. Anticipated performance of ASTER instrument in EM design phase, *Proc. SPIE*, 1939, 187-197.
- Gesch, D.B., and K.S. Larson, 1996. Techniques for development of global 1-kilometer digital elevation models. *Pecora Thirteen, Human Interactions with the Environment-Perspectives from Space*, (Sioux Falls, SD), August 20-22, 1996.
- Gillespie, A. R., 1987. Lithologic mapping of silicate rocks using TIMS data. *Proceedings of the Workshop on Thermal Infrared Multispectral Scanner* held at the Jet Propulsion Laboratory, Pasadena, CA USA, 1987, Jet Propulsion Laboratory Publication 36-38, pp. 29-44.
- Gillespie, A. R., Matsunaga, T., Rokugawa, S., and Hook, S. J., 1998. A Temperature and Emissivity Separation for Advanced Spaceborne Thermal Emission and Reflection Radiometer (ASTER) Images. *IEEE Transactions on Geoscience and Remote Sensing*, 36, 1113-1126.
- Gustafson, W. T., R. N. Handcock, A.R. Gillespie, and H. Tonooka, 2002. An image-sharpening method to recover stream temperatures from ASTEWR Images. *SPIE Workshop: Remote Sensing for Environmental Monitoring, GIS Applications, and Geology II*, Crete, Greece.
- Kahle, A.B., F.D. Palluconi, S.J. Hook, V.J. Realmuto and G. Bothwell. 1991. The Advanced Spaceborne Thermal Emission and Reflectance Radiometer (ASTER). *International Journal of Imaging Systems and Technology*, 3, 144-156.
- Kealy P. S. and S. Hook, 1993. Separating temperature and emissivity in thermal infrared multispectral scanner data: Implication for recovering land surface temperatures, *IEEE Transactions on Geoscience and Remote Sensing*, 31, 1155-1164.
- Matsunaga, T. 1994. A temperature-emissivity separation method using an empirical relationship between the mean, the maximum, and the minimum of the thermal infrared emissivity spectrum, in Japanese with English abstract, *J. Rem. Sens. Soc. Japan*, vol. 14, no. 2, pp. 230-241.
- Palluconi, F. D., G. Hoover, R. Alley and M. Jentoft-Nilsen, 1994. Atmospheric correction method for ASTER thermal radiometry over land, Algorithm Theoretical Basis Document, (Pasadena, CA: Jet Propulsion Laboratory).
- Sobrino J. A, N. Raissouni, and Z.-L. Li, 2001. A comparative study of land surface emissivity retrieval from NOAA data *Remote Sensing of Environment*, 75, 256-266.
- Thome, K., F. Palluconi, T. Takashima, and K. Masuda, 1998. Atmospheric correction of ASTER, *IEEE Transactions on Geoscience and Remote Sensing*, 36, 1199-1211.
- Tonooka, H., F. Sakuma, M. Kudoh, and K. Iwafune 2003. ASTER/TIR onboard calibration status and user-based recalibration, *Proc. SPIE*, 5234, 191-201.
- Yamaguchi, Y., H. Tsu and H. Fujisada, 1993. A scientific basis of ASTER instrument design, *Proc. SPIE*, 1939, 150-160.
- Young, S., B. Johnson, and J. Hackwell, 2002. An in-scene method for atmospheric compensation of thermal hyperspectral data, *J. Geo. Res.* 107(D24), 14-1-20.



Color Figure Caption. Spatial step discontinuities in a TES emissivity image of basalt flows from Mauna Loa on the island of Hawai'i (Figures 2 and 4, Gustafson et al. "Revisions to the ASTER temperature/emissivity separation algorithm"). Subsets are 64 90-m pixels (5.76 km) across. For the color composites, R G B = ASTER channels 10 (8.3 m), 12 (9.1 m), and 14 (9.1 m), respectively. MMD threshold value set to 0.032: a) Emissivity image. b) Subset from area of rectangle in a. c) Histogram of emissivities from the image subset. The gap and isolated spike in the histogram are due to the threshold test. MMD threshold value set to 0.00: d) Emissivity image. e) Subset from area of rectangle in d. f) Histogram of emissivities from the image subset.